Mesoporous silicon particles as a multistage delivery system for imaging and therapeutic applications

ENNIO TASCIOTTI[1], XUEWU LIU[1], ROHAN BHAVANE[1], KEVIN PLANT[1], ASHLEY D. LEONARD[2], B. KATHERINE PRICE[2], MARK MING-CHENG CHENG[1], PAOLO DECUZZI[3,4], JAMES M. TOUR[2], FREDIKA ROBERTSON[5] AND MAURO FERRARI[1,5,6]*

[1]Brown Foundation Institute of Molecular Medicine, The University of Texas Health Science Center at Houston, Houston, Texas 77030, USA
[2]Departments of Chemistry and Mechanical Engineering and Materials Science, and The Smalley Institute for Nanoscale Science and Technology, Rice University, Houston, Texas 77005, USA
[3]Center of BioNanotechnology and BioEngineering for Medicine, The University of Magna Graecia, Viale Europa – LOC. Germaneto 88100, Catanzaro, Italy
[4]School of Health Information Sciences, The University of Texas Health Science Center at Houston, Houston, Texas 77030, USA
[5]Department of Experimental Therapeutics, The University of Texas MD Anderson Cancer Center, Houston, Texas 77030, USA
[6]Department of Bioengineering, Rice University, Houston, Texas 77005, USA
*e-mail: mauro.ferrari@uth.tmc.edu

Published online: 2 March 2008; doi:10.1038/nnano.2008.34

Many nanosized particulate systems are being developed as intravascular carriers to increase the levels of therapeutic agents delivered to targets, with the fewest side effects[1,2]. The surface of these carriers is often functionalized with biological recognition molecules for specific, targeted delivery. However, there are a series of biological barriers in the body[3–5] that prevent these carriers from localizing at their targets at sufficiently high therapeutic concentrations[5,6]. Here we show a multistage delivery system that can carry, release over time and deliver two types of nanoparticles into primary endothelial cells. The multistage delivery system is based on biodegradable and biocompatible mesoporous silicon particles that have well-controlled shapes, sizes and pores. The use of this system is envisioned to open new avenues for avoiding biological barriers and delivering more than one therapeutic agent to the target at a time, in a time-controlled fashion.

Paradigmatic nanovectors for drug delivery include therapeutic or imaging contrast agents loaded within a carrier, which is decorated on its surface with biological recognition agents[5] such as antibodies[7], aptamers[8] or other ligands[9]. These systems are advantageous in specific applications. However, because of their size, composition, and charge, they interact imperfectly with the biological barriers that present themselves sequentially following injection[5]. These include enzymatic degradation[10], phagocytosis in peripheral blood and in the reticulo-endothelial system (RES)[11] and the crossing of the vascular endothelium. Margination and adhesion onto vascular endothelia are governed by haemodynamic forces that are effective barriers for injected agents[12,13]. The simultaneous attainment of preferential localization and avoidance of the sequential biological barriers is proving to be an exceedingly difficult problem in drug delivery. To overcome this problem, we hypothesized a multifunctional multistage delivery system (MDS) comprising stage 1 mesoporous particles (S1MPs) loaded with one or more types of stage 2 nanoparticles (S2NPs), which can in turn carry either active agents or higher-stage particles. By loading S2NPs inside the pores of the S1MPs, the enzymatic degradation and RES uptake of the S2NPs would be prevented. Design criteria based on mathematical modelling were used to yield S1MPs with optimal properties to increase margination to the vascular endothelium[13–15]. Future embodiments of the MDS are envisioned to integrate targeting moieties to localize the particles at desired sites and vascular penetration enhancers to increase the crossing of the endothelial barrier. In view of its biocompatibility[16–18], complete biodegradability[19] and previous successes with non-intravascular drug delivery macro-systems[20–22], mesoporous silicon was chosen as elective material for the production of S1MPs. S2NPs were quantum dots (Q-dots) and single-walled carbon nanotubes (SWNTs).

Figure 1a,b shows representative scanning electron micrograph (SEM) images of the back, front and cross-sections of large-pore (LP) and small-pore (SP) silicon S1MPs, respectively. Both types of particle were designed, engineered and fabricated to be highly porous and near hemispherical in shape (see Supplementary Information, Fig. S1). The diameter of the LP particles is $\sim$3.5 μm, with straight nanopores crossing the particles perpendicular to their external surface, with sizes ranging from 20 to 30 nm and a mean pore size of 24.2 nm, as determined by nitrogen adsorption–desorption volumetric isotherms (see Supplementary Information, Fig. S2a). The SP silicon particles have an approximate diameter of 3.2 μm, and have a flatter shape than the LP silicon particles as a consequence of the anodization and electropolishing processes used to produce them, with pore sizes ranging from 5 to 10 nm and a mean pore size of 7.4 nm (see Supplementary Information, Fig. S2b). Although non-oxidized silicon is hydrophobic, a variety of surface treatments can be used to stabilize and further functionalize silicon-based materials through a series of well-characterized techniques[23–25].

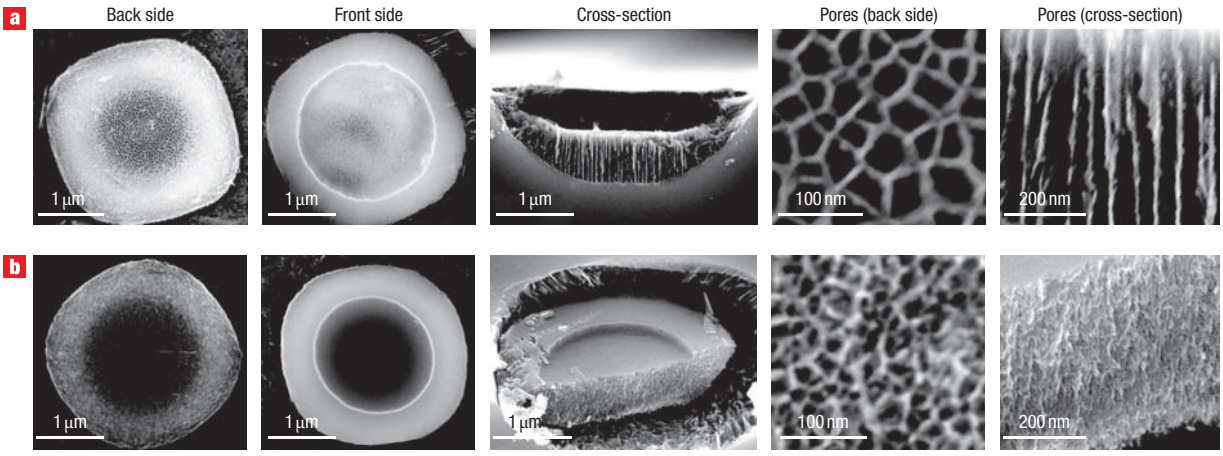

Figure 1 SEM images of a mesoporous silicon particle. a,**b**, Images of LP (**a**) and SP (**b**) particles. From left to right: back, front and cross-section of the particle; close-up view of the pores on the back side and cross-section. The overall sizes and shapes of the LP and SP particles are the same, but the size and structure of the pores are significantly different.

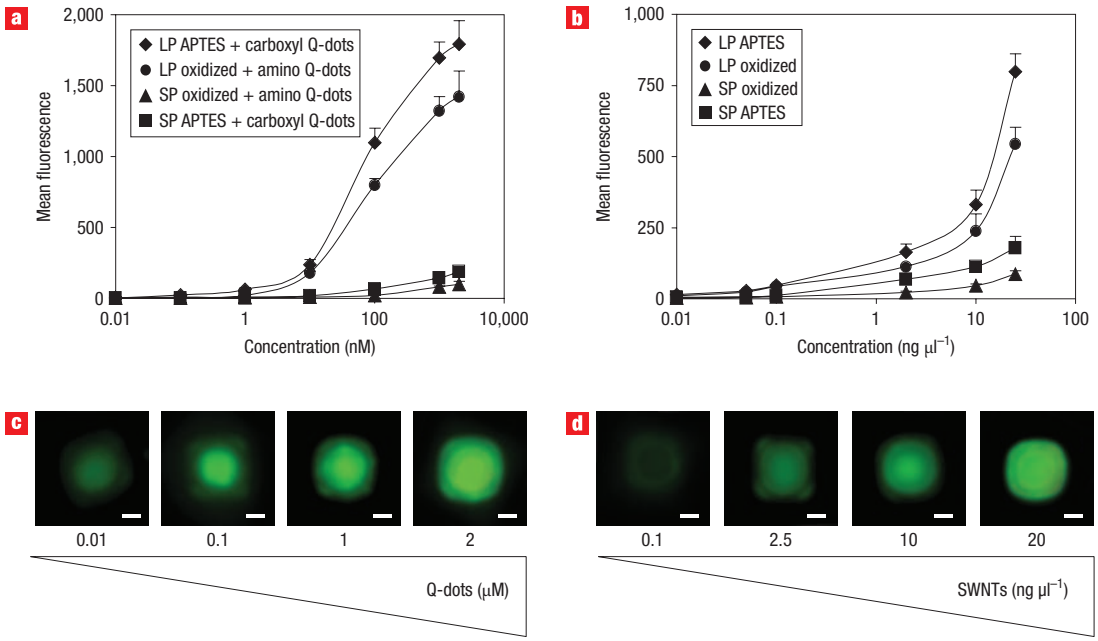

Figure 2 Flow cytometry and fluorescence microscopy of loading of Q-dots and PEG-FITC-SWNTs into mesoporous silicon. a,**b**, At the concentration used, loading of Q-dots (**a**) describes a sigmoidal curve, but loading of PEG-FITC-SWNTs (**b**) describes an exponential curve. Higher loading in the silicon particles results in higher mean fluorescence as measured by flow cytometry. In all graphs, error bars represent standard deviations. **c**,**d**, Fluorescence microscopy confirmed that when fewer Q-dots (**c**) and PEG-FITC-SWNTs (**d**) were used in the loading solution, the fluorescence decreased accordingly. White scale bars in **c** and **d** are 1 μm.

We modified the S1MPs, creating either positive or negative surface charges (see Supplementary Information, Fig. S3). All the S1MPs used in the study were biodegradable in saline and completely dissolved in orthosilicic acid in 24 h (see Supplementary Information, Fig. S4). The hydrodynamic sizes of the Q-dots and SWNTs linked to poly ethylene glycol (PEG)–fluorescein isothiocyanate (PEG-FITC-SWNTs) were established using dynamic light scattering and atomic force microscopy (AFM), respectively (see Supplementary Information, Fig. S5). We used the fluorescent properties of S2NPs to study and quantify loading and release from S1MPs through established techniques such as flow cytometry, fluorimetry, fluorescence and confocal microscopy (see Supplementary Information, Fig. S6), and developed protocols to efficiently load S2NPs inside the pores of the S1MPs (see Supplementary Information, Fig. S7, S8). We analysed the fluorescence intensity of S1MPs loaded with increasing amounts of Q-dots (Fig. 2a) and PEG-FITC-SWNTs (Fig. 2b), demonstrating, using flow cytometry, that loading was directly correlated to the concentration of the S2NPs (Fig. 2a,b) and by direct visualization with fluorescent microscopy (Fig. 2c,d) (see Supplementary Information, Fig. S9a,b). These studies also demonstrated that the chemical properties of the

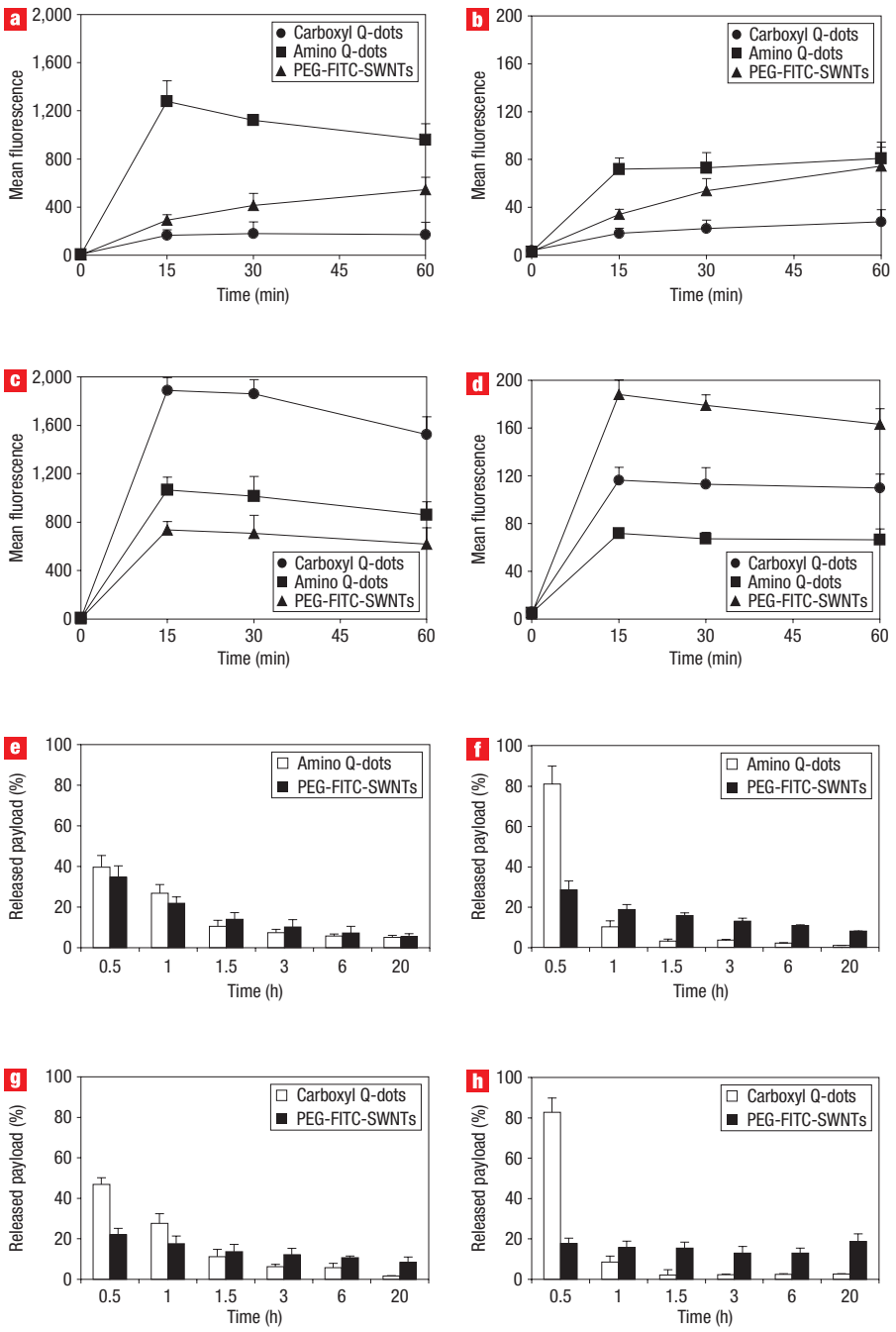

Figure 3 Time-dependent loading and release of S2NPs. a–d, Four different types of porous silicon particles were loaded with different S2NPs and their mean fluorescence measured by flow cytometry over time: LP oxidized (**a**), SP oxidized (**b**), LP APTES (**c**) and SP APTES (**d**). **e–h**, Release of Q-dots and PEG-FITC-SWNTs from LP oxidized (**e**), SP oxidized (**f**), LP APTES (**g**) and SP APTES (**h**) was measured over time and expressed as a percentage of the total amount of S2NP payload released from the S1MPs for every time interval, after optimal loading.

surfaces of both the S1MPs and S2NPs affected loading efficiency and stability of the assembled multistage nanoparticulate carrier system (see Supplementary Information, Fig. S9c,d). These observations were confirmed by the results shown in Fig. 3a and c. Carboxyl Q-dots, which had a negative surface charge (zeta potential, −32.8 mV), and PEG-FITC-SWNTs (zeta potential, −9.21 mV) could be loaded more efficiently into 3′-aminopropyltriethoxysilane (APTES)-modified LP (zeta potential, +6.52 mV) than into oxidized LP (zeta potential, −10.1 mV). Loading of S2NPs into S1MPs was generally very rapid (15 min) when the S1MPs and S2NPs had opposite electrostatic sign (Fig. 3a,c) and followed very reproducible regional patterns on the S1MPs according to the physical size of the pores and of the S2NPs (see Supplementary Information, Fig. S10). Owing to the physical constraints posed by the nanopores, loading of Q-dots and PEG-FITC-SWNTs into SP S1MPs was reduced to 6% and 25%, respectively (Fig. 3b,d; see also Supplementary Information, Fig. S9e,f).

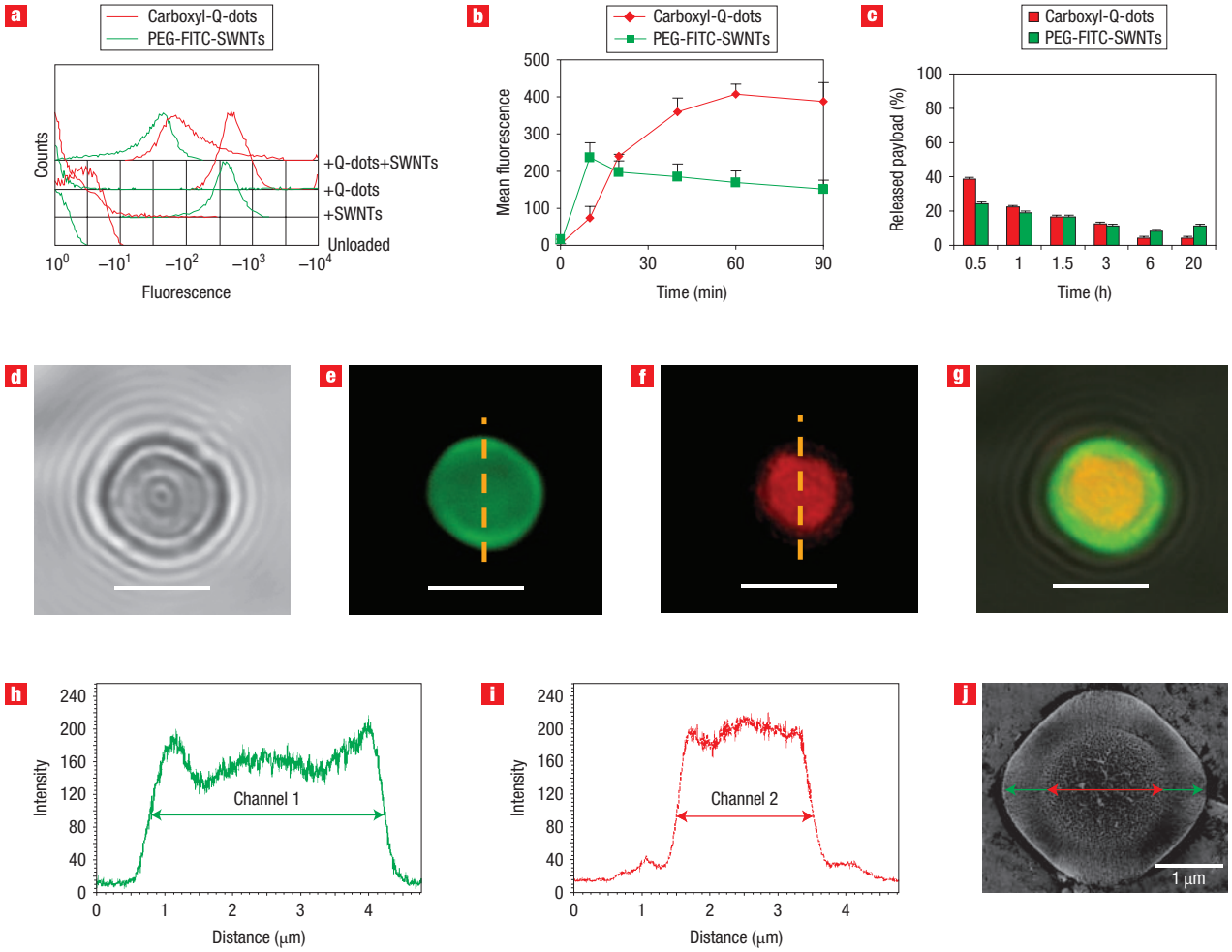

Figure 4 Simultaneous loading and release of Q-dots and PEG-FITC-SWNTs in porous silicon particles. a, FACS histogram overlay of LP APTES S1MPs (Unloaded); S1MPs loaded with PEG-FITC-SWNTs (+SWNTs), with Q-dots (+Q-dots) and with both Q-dots and SWNTs (+Q-dots + SWNTs). **b**,**c**, Flow cytometry analysis of simultaneous loading (**b**) and release (**c**) of S2NPs. **d**–**g**, Confocal microscopy images show the localization of PEG-FITC-SWNTs (green) and Q-dots (red) in a single porous silicon particle: bright-field (**d**), green (**e**) and red fluorescence (**f**) and overlay of the three channels (**g**) are shown. **h**,**i**, Fluorescence intensity profiles of each channel along the orange dashed lines in **e** (PEG-FITC-SWNTs) and **f** (Q-dots) are shown, respectively. **j**, The green and red arrows incorporated into the SEM image confirm the spatial distribution of fluorescence in S1MP. White scale bars in **d**–**g** are 3 μm.

We evaluated the release of S2NPs from S1MPs in physiologic conditions by performing all the experiments at 37 °C at pH 7.3 in a Tris-buffered saline and by replacing with fresh solution at each time point. We demonstrated that both types of S2NPs were released over time and that the process was sustained, with complete release reached after 20 h (Fig. 3e–h). The release kinetics of the Q-dots was significantly faster than that of PEG-FITC-SWNTs. As an example, 80% of the Q-dots payload was released in the first 1.5 h, compared to just 50% of the PEG-FITC-SWNTs released at the same time point (P-value <0.05) (Fig. 3g).

To demonstrate the versatility of the MDS, we simultaneously loaded both red fluorescent Q-dots (emission 565 nm) and green fluorescent PEG-FITC-SWNTs (emission 510 nm) into S1MPs. Both types of S2NPs could be loaded into the same S1MP carriers (Fig. 4a). The dynamics of multiple loading were different from those described for single loading and reached a stable plateau after 60 min (Fig. 4b). On the contrary, the release profiles of S2NPs (Fig. 4c) were unaltered compared with those of Fig. 3e,g. The confocal microscopy images shown in Fig. 4d–g demonstrate that each S2NP type preferentially localized to a specific area of the silicon particle. The profiles in Fig. 4h,i show a representative example of the fluorescence intensity of PEG-FITC-SWNTs and Q-dots for comparison with Fig. 4e,f. respectively. Given their larger size, Q-dots were exclusively found in the central area in association with the larger pores of the S1MP (Fig. 4i,j). PEG-FITC-SWNTs were found throughout the entire S1MP, with their primary accumulation along the borders of the particle (Fig. 4h,j). When S1MPs loaded with S2NPs were incubated with cultured human umbilical vein endothelial cells (HUVEC), S2NPs were released and selectively internalized by the cells. Both Q-dots (Fig. 5a,b) and PEG-FITC-SWNTs (Fig. 5c,d) entered the cytosol and accumulated inside distinct vesicles. Internalization of Q-dots and PEG-FITC-SWNTs occurred with similar kinetics and potentially through the same mechanisms as suggested by the co-localization of the fluorescent signals (Fig. 5e–g). The bright-field images in Fig. 5b,d,g show the details of particle morphology, suggesting that, at this time point, the S1MPs were associated with the external cell surface rather than being internalized by HUVECs, as confirmed by confocal imaging

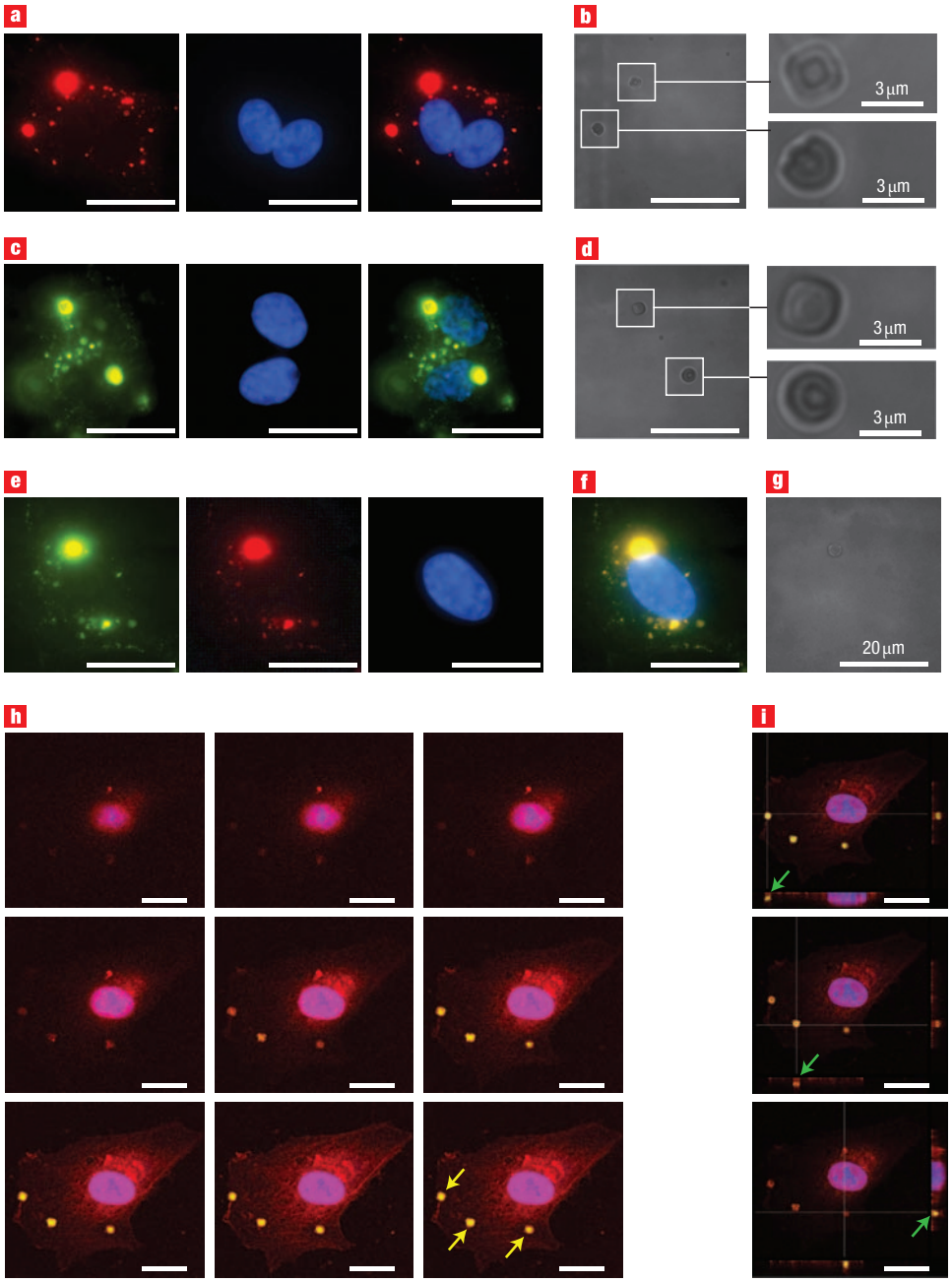

Figure 5 Intracellular internalization of S2NPs delivered by S1MPs. a–g, Fluorescence microscope images of cells incubated for 30 min with S1MPs loaded with Q-dots (**a**,**b**); PEG-FITC-SWNTs (**c**,**d**) or both Q-dots and SWNTs (**e–g**). Insets in **b** and **d** show bright-field magnifications of S1MP morphology. **h**, Confocal images of a cell incubated with FITC-labelled S1MPs. The series of different focal planes acquired through the sample (Z-stack) shows that the particles (yellow arrows) are on the cell surface. **i**, Orthogonal projections of the Z-stack reconstructions, showing relative position of particles (green arrows) compared to the cell body (red staining is actin, blue staining is nuclear DNA). White scale bars in **a–i** are 20 μm unless otherwise indicated.

(Fig. 5 h,i; see also Supplementary Information, Fig. S11). Cells grown in the presence of S1MPs did not show either abnormal morphological changes (see Supplementary Information, Fig. S12) or variation of the proliferation rates (see Supplementary Information, Fig. S13) over time.

Our studies provide an intravascular MDS, with mesoporous silicon particles as the first stage. We have demonstrated the loading, controlled release and simultaneous *in vitro* delivery of Q-dots and SWNTs to human vascular cells.

In future developments, based on mathematical methods of rational design[26] (see Supplementary Information, Results and Discussion and Fig. S14), S1MPs are envisioned to transport and protect a payload of nanoparticles and bioactive agents throughout the journey within the circulatory system[13]. The endothelium-localized S2NP and higher-stage nanoparticles will deliver drug molecules and contrast agents directly to extravascular target tumour cells. In this respect their choice and design should optimize crossing of the endothelial barrier,

either passively through intravascular gaps and fenestrations or actively exploiting cellular transcytotic mechanisms, and transport within the extravascular compartment. The penetration of the active payloads through the vascular endothelium may be facilitated by permeation enhancers co-delivered with the S2NPs at the target vascular location (see Supplementary Information, Fig. S15).

Given the wide range of protocols available to modify porous silicon[16,23–25], several different S2NPs can be efficiently loaded by tailoring first- and second-stage surface chemistries. Future developments will focus on the co-delivery of therapeutic nanovectors (liposomes[27], gold nanoshells[28] and microbots[29]) and imaging contrast nanoparticles (Q-dots[30], iron oxide[31] and SWNTs[32]). This will allow the development of a large combinatorial library of multistage vectors in which multiple therapeutic and imaging agents can be simultaneously administered at the systemic level. These vectors will have the ability to circumvent the biological barriers, thus resulting in simultaneous and efficient localization of various agents at the target sites.

METHODS

FABRICATION OF POROUS SILICON PARTICLES

A heavily doped p^{++} type Si(100) wafer with a resistivity of 0.005 Ω cm^{-1} (Silicon Quest) was used as the substrate. A 200-nm layer of silicon nitride was deposited by a low-pressure chemical vapour deposition system. Standard photolithography was used to pattern using a EVG 620 contact aligner. LP S1MPs were formed in a mixture of hydrofluoric acid (HF) and ethanol (3:7 v/v) by applying a current density of 80 mA cm^{-2} for 25 s. A high-porosity layer was formed by applying a current density of 320 mA cm^{-2} for 6 s in a 49% hydrofluoric acid (HF):ethanol mixture with a ratio of of 2:5 (v/v). The LP S1MPs were formed in a mixture of HF (49%) and ethanol (3:7 v/v) by applying a current density of 80 mA cm^{-2} for 25 s. The SP S1MPs were formed in a mixture of HF (49%) and ethanol (1:1 v/v) by applying a current density of 6 mA cm^{-2} for 1.75 min. After removing the nitride layer by HF, particles were released by ultrasound in isopropyl alcohol for 1 min.

LOADING OF Q-DOTS AND SWNTs INTO S1MPs

The S1MPs that were used in the development of the MDS include oxidized and APTES-modified LP and SP particles. The S2NPs include amino-PEG Q-dots, carboxyl Q-dots and PEG-FITC-SWNTs. To optimize loading of the S2NPs into the S1MPs, 3.0×10^5 silicon particles were resuspended in low-binding polypropylene centrifuge tubes (VWR International) containing 3 μl of deionized water. Tris(hydroxymethyl)aminomethane (Tris-HCl) solution was adjusted to the right molarity at pH 7.3. Either 2 μM Q-dots (5 μl) or 20 ng μl^{-1} PEG-FITC-SWNTs (9 μl) were added to the Tris-HCl solution, with 20 μl as the final volume. Samples were incubated on a rotating wheel (20 r.p.m.) for 15 min at 25 °C. After incubation, the samples were diluted with 20 mM Tris-HCl, pH 7.3, to a volume of 150 μl and promptly examined for fluorescence intensity using a FACScalibur (Becton Dickinson) flow cytometer. To evaluate the concentration-dependent loading of Q-dots and PEG-FITC-SWNTs into silicon particles, we used 3.0×10^5 silicon particles and an incubation time of 15 min, with either 0.01, 0.1, 1, 10, 100, 1,000 or 2,000 nM Q-dots or 0.05, 0,1, 2.5, 10 or 20 ng μl^{-1} PEG-FITC-SWNTs. To evaluate the time-dependent loading, we used 3.0×10^5 first-stage particles, 2,000 nM Q-dots or 20 ng μl^{-1} PEG-FITC-SWNTs with incubation times of 15, 30, 45 and 60 min. For evaluation of loading of silicon particles with both Q-dots and PEG-FITC-SWNTs, 3.0×10^5 silicon particles, 1,000 nM Q-dots and 10 ng μl^{-1} PEG-FITC-SWNTs were used with the same final volume of incubation.

RELEASE OF Q-DOTS AND SWNTs FROM S1MPs

LP-oxidized or APTES-modified S1MPs (2.1×10^6) were combined with 2 μM amino-PEG Q-dots or carboxyl Q-dots in a 200 mM Tris-HCl solution at pH 7.3 or with 20 ng μl^{-1} PEG-FITC-SWNTs in a 20 mM Tris-HCl solution at pH 7.3 or with both 1 μM Q-dots and 10 ng μl^{-1} PEG-FITC-SWNTs in a 50 mM Tris-HCl solution at pH 7.3 to a final incubation volume of 140 μl. Samples were incubated on a rotating wheel (20 r.p.m.) for 15 min at 25 °C, washed in 1.4 ml deionized water and centrifuged for 5 min at 4,200 r.p.m. in a Beckman Coulter Allegra X-22 centrifuge. Pellets were resuspended in 70 μl deionized water and 10 μl were removed from each vial to assess the fluorescence of the samples using flow cytometry. Fluorescence was recorded at time 0 and then over six time points, 30, 60, 90, 180, 360 and 1,200 min. The residual 60 μl left in each vial was diluted to 3 ml with 20 mM Tris-HCl 0.9% NaCl release buffer, followed by incubation at 37 °C on a rotating wheel (20 r.p.m.) for the given amount of time. At each time point, samples were centrifuged for 5 min at 4,200 r.p.m. and the fluorescence evaluated using flow cytometry.

SILICON PARTICLE INCUBATION WITH CELLS

HUVEC cells were seeded into BD Falcon four-well chamber CultureSlides (BD Biosciences) and kept in culture in standard conditions until 50% confluency was reached. Loaded S1MPs (4×10^5) were added (cell:particle ratio 1:2) and incubated for 30 min. Samples were fixed with 4% methanol-free paraformaldehyde for 10 min, permeabilized in 0.1% Triton-X 100 in PBS for 3 min, mounted and analysed. For confocal microscopy, cells were incubated with FITC-conjugated particles as already described. After fixation and permeabilization, cells were washed with PBS, blocked in 1.0% bovine serum albumin in PBS for 10 min, and stained with a solution containing 0.5 unit μl^{-1} Alexa Fluor 555-conjugated phallodin (Molecular Probes, Invitrogen) for 30 min at room temperature. DNA was visualized through TOTO3 staining (Molecular Probes).

Received 27 September 2007; accepted 7 February 2008; published 2 March 2008.

References

1. Brannon-Peppas, L. & Blanchette, J. O. Nanoparticle and targeted systems for cancer therapy. *Adv. Drug Deliv. Rev.* **56,** 1649–1659 (2004).
2. Yezhelyev, M. V. *et al.* Emerging use of nanoparticles in diagnosis and treatment of breast cancer. *Lancet Oncol.* **7,** 657–667 (2006).
3. Ferrari, M. Nanovector therapeutics. *Curr. Opin. Chem. Biol.* **9,** 343–346 (2005).
4. Sakamoto, J., Annapragada, A., Decuzzi, P. & Ferrari, M. Antibiological barrier nanovector technology for cancer applications. *Expert Opin. Drug Deliv.* **4,** 359–369 (2007).
5. Ferrari, M. Cancer nanotechnology: opportunities and challenges. *Nature Rev. Cancer* **5,** 161–171 (2005).
6. Eckelman, W. C. & Mathis, C. A. Targeting proteins *in vivo*: *In vitro* guidelines. *Nucl. Med. Biol.* **33,** 161–164 (2006).
7. Lin, M. Z., Teitell, M. A. & Schiller, G. J. The evolution of antibodies into versatile tumor-targeting agents. *Clin. Cancer Res.* **11,** 129–138 (2005).
8. Farokhzad, O. C., Karp, J. M. & Langer, R. Nanoparticle–aptamer bioconjugates for cancer targeting. *Expert Opin. Drug Deliv.* **3,** 311–324 (2006).
9. Torchilin, V. P. Multifunctional nanocarriers. *Adv. Drug Deliv. Rev.* **58,** 1532–1555 (2006).
10. Shuvaev, V. V. *et al.* Factors modulating the delivery and effect of enzymatic cargo conjugated with antibodies targeted to the pulmonary endothelium. *J. Controlled Release* **118,** 235–244 (2007).
11. Medina, O. P., Zhu, Y. & Kairemo, K. Targeted liposomal drug delivery in cancer. *Curr. Pharm. Des.* **10,** 2981–2989 (2004).
12. Pierres, A., Benoliel, A.-M., Zhu, C. & Bongrand, P. Diffusion of microspheres in shear flow near a wall: use to measure binding rates between attached molecules. *Biophys. J.* **81,** 25–42 (2001).
13. Decuzzi, P., Lee, S., Bhushan, B. & Ferrari, M. A theoretical model for the margination of particles within blood vessels. *Ann. Biomed. Eng.* **33,** 179–190 (2005).
14. Decuzzi, P. F. & Ferrari, M. Fantastic voyages. *Mech. Eng.* **128,** 24–27 (2006).
15. Decuzzi, P., Lee, S., Decuzzi, M. & Ferrari, M. Adhesion of microfabricated particles on vascular endothelium: a parametric analysis. *Ann. Biomed. Eng.* **32,** 793–802 (2004).
16. Canham, L. T. *et al.* Derivatized mesoporous silicon with dramatically improved stability in simulated human blood plasma. *Adv. Mater.* **11,** 1505–1507 (1999).
17. Bayliss, S. C., Heald, R., Fletcher, D. I. & Buckberry, L. D. The culture of mammalian cells on nanostructured silicon. *Adv. Mater.* **11,** 318–321 (1999).
18. Chin, V., Collins, B. E., Sailor, M. J. & Bhatia, S. N. Compatibility of primary hepatocytes with oxidized nanoporous silicon. *Adv. Mater.* **13,** 1877–1880 (2001).
19. Canham, L. T. Bioactive silicon structure fabrication through nanoetching techniques. *Adv. Mater.* **7,** 1033–1037 (1995).
20. Foraker, A. B. *et al.* Microfabricated porous silicon particles enhance paracellular delivery of insulin across intestinal caco-2 cell monolayers. *Pharm. Res.* **20,** 110–116 (2003).
21. Salonen, J. *et al.* Mesoporous silicon microparticles for oral drug delivery: Loading and release of five model drugs. *J. Controlled Release* **108,** 362–374 (2005).
22. Thomas, J. C., Pacholski, C. & Sailor, M. J. Delivery of nanogram payloads using magnetic porous silicon microcarriers. *Lab Chip* **6,** 782–787 (2006).
23. Stewart, M. P. & Buriak, J. M. Chemical and biological applications of porous silicon technology. *Adv. Mater.* **12,** 859–869 (2000).
24. Song, J. H. & Sailor, M. J. Chemical modification of crystalline porous silicon surfaces. *Comments Inorg. Chem.* **21,** 69–84 (1999).
25. Wang, Y. & Ferrari, M. Surface modification of micromachined silicon filters. *J. Mater. Sci.* **35,** 4923–4930 (2000).
26. Decuzzi, P. & Ferrari, M. The adhesive strength of non-spherical particles mediated by specific interactions. *Biomaterials* **27,** 5307–5314 (2006).
27. Lasic, D. D., Martin, F. J., Gabizon, A., Huang, S. K. & Papahadjopoulos, D. Sterically stabilized liposomes: a hypothesis on the molecular origin of the extended circulation times. *Biochim. Biophys. Acta.* **1070,** 187–192 (1991).
28. Hirsch, L. R. *et al.* Nanoshell-mediated near-infrared thermal therapy of tumours under magnetic resonance guidance. *Proc. Natl Acad. Sci. USA* **100,** 13549–13554 (2003).
29. Akin, D. *et al.* Bacteria-mediated delivery of nanoparticles and cargo into cells. *Nature Nanotechn.* **2,** 441–449 (2007).
30. Kim, S. *et al.* Near-infrared fluorescent type II quantum dots for sentinel lymph node mapping. *Nature Biotechnol.* **22,** 93–97 (2004).

31. Corot, C., Robert, P., Idee, J.-M. & Port, M. Recent advances in iron oxide nanocrystal technology for medical imaging. *Adv. Drug Deliv. Rev.* **58,** 1471–1504 (2006).
32. Kam, N. W. S., O'Connell, M., Wisdom, J. A. & Dai, H. Carbon nanotubes as multifunctional biological transporters and near-infrared agents for selective cancer cell destruction. *Proc. Natl Acad. Sci. USA* **102,** 11600–11605 (2005).

Acknowledgements

We thank the University of Texas at Austin for the use of the semiconductor cleanroom facilities, M. Landry for excellent graphical support, A. Jimenez for laboratory assistance, and T. Tanaka and B. Godin for helpful suggestions. These studies were supported by the following grants: DoDW81XWH-04-2-0035 Project 16 (M.F., M.C., X.L., E.T., R.B.), NASA SA23-06-017 (M.F., M.C., X.L., R.B., E.T., J.T., A.L., B.K.P.), State of Texas, Emerging Technology Fund (M.F., X.L., R.B., K.P.), and the National Institutes of Health (NIH) NCI 1R21CA1222864-01 (M.F., M.C., F.R.). The authors would like to recognize the contributions and support from the Alliance for NanoHealth (ANH).
Correspondence and requests for materials should be addressed to M.F.
Supplementary information accompanies this paper on www.nature.com/naturenanotechnology.

Author contributions

E.T. and M.F. conceived and designed all the experiments. E.T. and K.P. performed the loading and release experiments. E.T. performed the fluorescence and confocal microscopy, the multiple loading and releasing experiments and the delivery experiments on HUVEC cells. R.B. made the chemical modifications to particles and measured the zeta potential values. X.L. and M.C. made the porous silicon particles, conducted the SEM imaging and the BET analysis. A.L. and B.K.P. made and characterized the PEG-FITC-SWNTs under the guidance of J.T.. P.D. developed the mathematical modeling and E.T., M.F. and F.R. discussed the interpretation of results. E.T. wrote the draft paper and all co-authors helped in the revision of the paper.

Competing financial interests

The authors declare competing financial interests: details accompany the full-text HTML version of the paper at www.nature.com/naturenanotechnology.